BIOCHEMISTRY
including biophysical chemistry & molecular biology

ARTICLE

pubs.acs.org/biochemistry

Proton-Coupled Electron Transfer in the Catalytic Cycle of *Alcaligenes xylosoxidans* Copper-Dependent Nitrite Reductase

Nicole G. H. Leferink,[†] Cong Han,[‡] Svetlana V. Antonyuk,[‡] Derren J. Heyes,[†] Stephen E. J. Rigby,[†] Michael A. Hough,[‡] Robert R. Eady,[‡] Nigel S. Scrutton,[*,†] and S. Samar Hasnain[*,‡]

[†]Manchester Interdisciplinary Biocentre and Faculty of Life Sciences, University of Manchester, Manchester M1 7DN, United Kingdom

[‡]Molecular Biophysics Group, Institute of Integrative Biology, Faculty of Health and Life Sciences, University of Liverpool, Liverpool L69 7ZB, United Kingdom

Supporting Information

ABSTRACT: We demonstrated recently that two protons are involved in reduction of nitrite to nitric oxide through a proton-coupled electron transfer (ET) reaction catalyzed by the blue Cu-dependent nitrite reductase (Cu NiR) of *Alcaligenes xylosoxidans* (*Ax*NiR). Here, the functionality of two putative proton channels, one involving Asn90 and the other His254, is studied using single (N90S, H254F) and double (N90S−H254F) mutants. All mutants studied are active, indicating that protons are still able to reach the active site. The H254F mutation has no effect on the catalytic activity, while the N90S mutation results in ∼70% decrease in activity. Laser flash-photolysis experiments show that in H254F and wild-type enzyme electrons enter at the level of the T1Cu and then redistribute between the two Cu sites. Complete ET from T1Cu to T2Cu occurs only when nitrite binds at the T2Cu site. This indicates that substrate binding to T2Cu promotes ET from T1Cu, suggesting that the enzyme operates an ordered mechanism. In fact, in the N90S and N90S−H254F variants, where the T1Cu site redox potential is elevated by ∼60 mV, inter-Cu ET is only observed in the presence of nitrite. From these results it is evident that the Asn90 channel is the main proton channel in *Ax*NiR, though protons can still reach the active site if this channel is disrupted. Crystallographic structures provide a clear structural rationale for these observations, including restoration of the proton delivery via a significant movement of the loop connecting the T1Cu ligands Cys130 and His139 that occurs on binding of nitrite. Notably, a role for this loop in facilitating interaction of cytochrome c_{551} with Cu NiR has been suggested previously based on a crystal structure of the binary complex.

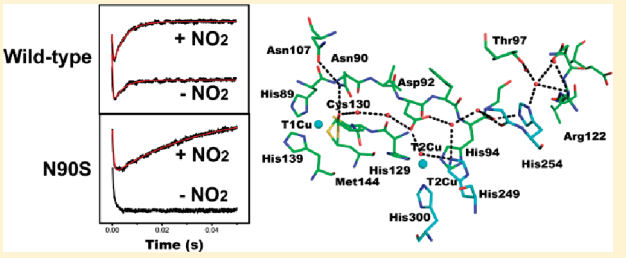

Nitrite reductases (NiRs) catalyze the one-electron reduction of nitrite (NO_2^-) into gaseous nitric oxide (NO), which is the first committed step in microbial denitrification:

$$NO_2^- + 2H^+ + e^- \rightarrow NO + H_2O \quad (1)$$

During denitrification fixed nitrogen is removed from the biosphere by the sequential reduction of nitrate (NO_3^-) to nitrogen gas, via the intermediates NO_2^-, NO, and nitrous oxide (N_2O).[1] Two classes of periplasmic NiRs can be distinguished in denitrifying bacteria: one containing heme cd_1 as prosthetic groups and a second containing two types of copper centers. The Cu NiRs have type 1 redox active Cu centers and a type 2 Cu catalytic site.[2] The intensively studied Cu-containing enzymes are homotrimers and can be divided into two distinct subclasses based on their color, blue or green. Atomic resolution crystal structures are available for both subclasses of copper-dependent NiRs.[3,4] Cu NiRs receive electrons from an external electron donor protein, which can be small Cu-containing or heme-containing proteins.[2] More recently, two new classes of Cu NiRs have been recognized with a similar trimeric architecture but with an additional cupredoxin or heme *c*-containing domain.[5,6]

NiR from *Alcaligenes xylosoxidans* (*Ax*NiR) contains two copper centers per monomer: a blue type 1 copper (T1Cu) which receives electrons from the external electron donor and an essentially colorless type 2 copper (T2Cu) center which is part of the active site where nitrite is reduced. The T1Cu is buried about 7 Å beneath the protein surface and is coordinated by two histidine residues, a cysteine residue, and a methionine residue. The T2Cu is located at the monomer−monomer interface and is coordinated by three histidine residues, originating from two distinct monomers, and a water molecule. The two copper centers are connected via a 12.5 Å long bridge, consisting of the T1Cu-coordinating Cys and one of the T2Cu His ligands, which together form the internal electron transfer (ET) pathway[4,7] (Figure 1). The reaction catalyzed by *Ax*NiR involves the controlled delivery of protons and electrons to the active site where substrate is utilized. The reaction mechanism has been studied intensively, but the exact order of events is still under

Received: February 17, 2011
Revised: April 3, 2011
Published: April 07, 2011

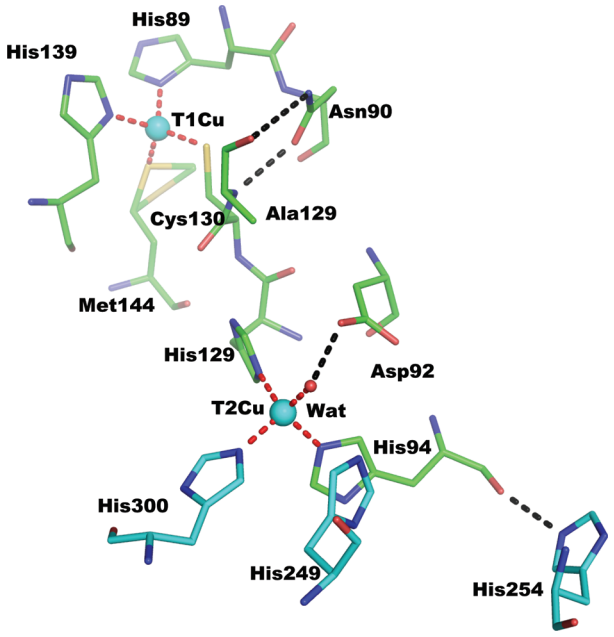

Figure 1. Structure of the type 1 and type 2 Cu sites in copper nitrite reductase, the links between them, and residues involved in putative proton transfer pathways, generated from pdb entry 1oe1. Residues originating from an adjacent monomer in the crystallographic asymmetric unit are shown in blue, Cu ions are shown as cyan spheres, and a water molecule is a smaller red sphere.

debate.[8−11] The proposed mechanisms for Cu-dependent NiR involve the binding of nitrite to the T2Cu center upon which bound water is displaced, ET from the reduced T1Cu to T2Cu, and proton transfer from Asp92 to bound nitrite forming a Cu^{+}−NOOH intermediate. His249 donates the second proton; the O−NO bond is cleaved to form the product NO, which dissociates to leave bound water to the oxidized T2Cu.[10] Nitrite binding and the inter-Cu ET have been studied intensively by pH-dependent and pulsed-radiolysis studies,[12−15] but the timing of the delivery and origin of protons remains unclear, although computational and pH drop experiments implicate delivery of a proton from Asp in triggering ET to the nitrite-bound T2Cu site.[16] Brenner et al. have shown that the one-electron reduction of nitrite involves the consumption of two protons, originating from the bulk solvent, and provided the first evidence for proton-coupled ET in *Ax*NiR.[17]

In the atomic resolution crystal structures of *Ax*NiR two putative proton channels were identified connecting the active site residue Asp92 to the surface of the protein.[4,18,19] The first channel connects Asp92 to the surface of the protein via Asn90 and several other residues and water molecules.[19] The second channel extends along the monomer−monomer interface via His254, which is proposed to regulate the proton flow.[18] Both these networks are conserved among copper-dependent NiRs and were also observed in the subatomic resolution crystal structure of the green NiR from *Achromobacter cycloclastes*.[3] The hydrogen-bonding networks in both channels were disrupted previously by mutation of His254 to Phe in the first channel and Asn90 to Ser in the second channel in *Ax*NiR.[9] Crystal structures of both single mutants clearly showed disruption of the hydrogen-bonding networks. The H254F mutation results in a variant that preferentially incorporates Zn at the T2Cu site but has no effect on the catalytic activity if corrected for T2Cu occupancy. The N90S mutation yields a significant (70%) reduction in catalytic activity.[9]

Here we present a detailed kinetic and functional analysis of the properties of both the *Ax*NiR N90S and H254F single mutants and the newly created N90S−H254F double mutant as well as the crystal structures of the double mutant, nitrite-soaked recombinant native NiR (native + NO_2^-), and nitrite-soaked N90S mutant (N90S + NO_2^-). Our work provides for better understanding of the role of the individual proton channels and the mechanism of proton-coupled ET in copper-dependent NiRs.

EXPERIMENTAL PROCEDURES

Protein Production and Sample Handling. Recombinant native and the N90S and H254F mutants of NiR from *A. xylosoxidans* (*Ax*NiR) were expressed and purified essentially as previously described.[9,17] The N90S−H254F double mutant was produced using the Quikchange mutagenesis protocol (Stratagene) as described previously.[9] Samples for kinetic experiments were prepared and handled anaerobically, and copper content was estimated using a spectrophotometric method (see Supporting Information).

Multiple Turnover Experiments. Proton counting experiments using the pH indicator phenol red were performed in a glovebox in unbuffered solution (110 mM KCl) as described before.[17]

The steady-state NiR enzyme activity was measured in a stopped-flow instrument (Applied Photophysics SC18MV) using deoxyhemoglobin as NO scavenger as described before.[17] All measurements were carried out in 50 mM potassium phosphate buffer, pH 7 at 4 °C. Initial rates were determined from the slopes of the progress curves and converted to units of activity by dividing through a calibration factor of 0.0162 ΔA430 μM^{-1} obtained in a calibration experiment using limited nitrite concentrations. Data were fitted using Origin software (OriginLab).

Laser-Flash Photolysis. Laser-flash photolysis experiments were essentially carried out as described before.[17] Briefly, cuvettes containing 30 μM NiR, 200 μM NADH, 50 mM *N*-methyl nicotinamide, and various concentrations of potassium nitrite in 50 mM potassium phosphate buffer, pH 7.0 (final volume of 500 μL), were filled in a glovebox, sealed with a rubber seal, and taken out of the box for laser analysis. All laser experiments were performed at 4 °C. The samples were excited at 355 nm using the third harmonic of a Q-switched Nd:YAG laser (Brilliant B, Quantel). Spectral transients were collected at 595 nm for up to 50 ms using an Applied Photophysics LKS-60 flash photolysis instrument as reported before.[17] Data were fitted using Origin software.

Reduction Potentials. Electrochemical titrations to determine the reduction potentials of both copper centers were performed as described previously.[20] Protein solutions (33 μM NiR, equivalent to 100 μM T2Cu) were titrated with sodium dithionite as the reductant. Mediators [phenazine methosulphate (2 μM), methyl viologen (0.5 μM), and benzyl viologen (1 μM)] were added to facilitate electrical communication between enzyme and electrode, prior to titration. The electrode potential was allowed to stabilize between each addition. The optical absorbance at 595 nm of oxidized type 1 copper was monitored at each potential using a Cary UV-50 Bio UV−vis scanning spectrophotometer. The electrochemical potential of the solution was measured using a Mettler Toledo SevenEasy pH meter coupled to a Pt/Calomel electrode (ThermoRussell Ltd.) at 25 °C. The electrode was calibrated using the Fe^{3+}/Fe^{2+} EDTA couple as a standard. A factor of 244 mV was used to correct relative to the standard hydrogen electrode. During the spectroelectrochemical titrations with dithionite, samples

Table 1. Data Collection and Refinement Statistics

name of sample	N90S−H254F	native + NO_2^-	N90S + NO_2^-	H254F[a]	N90S[a]
resolution (last shell) (Å)	23−1.46 (1.51−1.46)	40−2.34 (2.43−2.34)	43.7−3.0 (3.17−3.0)	26.0−1.50 (1.54−1.5)	23−1.60 (1.64−1.6)
no. of unique reflections	146 766	232 959	109 627	126 006	101 151
symmetry	*R*3	$P2_12_12_1$	$P2_12_12_1$	*R*3	*R*3
completeness (last shell) (%)	99.1 (91.0)	99.4 (96.7)	99.3 (98.3)	97.1 (78.2)	93.8 (60.6)
multiplicity (last shell)	4.2 (2.9)	7.1 (6.9)	4.8 (4.7)	3.2 (3.0)	2.5 (2.2)
$\langle I\rangle/\sigma(I)$	12.9 (1.8)	9.6 (1.7)	20.4 (2.54)	18.9 (2.95)	12.0 (2.10)
R_{merge} (%)	9.0 (68.0)	12.4 (54.0)	8.4 (86.1)	4.8 (27.0)	7.2 (32.9)
Wilson *B*-factor (Å^2)	11.8	60.7	62.0	25.0	19.0
unit cell (Å)					
a	89.24	173.93	172.65	89.3	89.6
b	89.24	176.82	174.64	89.3	89.6
c	288.27	181.59	180.64	287.9	287.7
R_{cryst} (R_{free}) (%)	12.5 (15.0)	17.4 (19.9)	18.7 (22.1)	14.7 (17.6)	16.8 (21.0)
mean *B*-factor (Å^2)	17.1	31.8	68.0	19.2	17.2
rms deviations					
bond distances (Å)	0.017	0.016	0.011	0.017	0.015
bond angles (deg)	1.797	1.594	1.369	1.937	1.836
estimated overall coordinate error (Å)	0.05	0.014	0.348	0.064	0.098
non-hydrogen atoms*	6071	17 342	15 716	5903	5904
solvent atoms	694	1571	156	573	680
PDB accession number	2xx0	2xwz	2xx1	2xxf	2xxg

[a] These columns refer to re-refinements of our earlier structures[9] using the latest software in order to ensure consistency with the new structures. The resolution of the data was set to include weaker but significant data according to the following criteria; i.e., data completeness in the last shell is better than 70%, $I/\sigma(I)$ is better than 1.5, and redundancy is better then 2.0. Inclusion of these data were finally assessed by monitoring the *R*-factor and R_{free} in the highest resolution shell and final resolution was set to when *R*-factor in the last shell became 35%. For native + NO_2 and N90S + NO_2^-, the values of highest resolution shell *R*-factor/R_{free} were 31/34 and 30/34%, respectively.

(250 μL) were withdrawn for electron paramagnetic resonance (EPR) spectroscopic analysis. The samples were placed in 4 mm Suprasil quartz EPR tubes supplied by Wilmad and sealed inside the glovebox, where they were immediately removed and frozen in liquid nitrogen. Samples were stored in liquid nitrogen to prevent reoxidation until they were analyzed. EPR spectra were recorded at 20 ± 0.1 K on a Bruker ELEXSYS E500/E580 EPR spectrometer (Bruker GmbH) fitted with an Oxford Instruments ESR900 helium flow cryostat coupled to a ITC 503 controller from the same manufacturer. The microwave power was 0.5 mW, the modulation frequency 100 kHz, and the modulation amplitude 5 G. The *g* values given and the integrals of the T2Cu hyperfine peaks were calculated using the software package supplied with the instrument.

Crystallization, Data Collection, Structure Solution, and Refinement. Crystals for the N90S−H254F, native + NO_2^-, and N90S + NO_2^- structures of NiR were grown using the hanging drop vapor diffusion method at room temperature. For the double mutant 2 μL of 10 mg/mL protein solution in 20 mM Tris-HCl (pH 7.4) was mixed with an equal volume of reservoir solution containing 20% PEG550 MME, 50 mM $ZnSO_4$, and 100 mM MES buffer (pH 6.5). For native and N90S crystals 5 μL of 10 mg/mL protein solution in 20 mM Tris-HCl (pH 7.4) was mixed with an equal volume of reservoir solution containing 1.8 M lithium sulfate in Na-acetate buffer, pH 4.25, and 1.8 M ammonium sulfate in citrate buffer, pH 4.6, respectively. Crystals grew within 1 week. Prior to being frozen in liquid nitrogen double mutant crystals were transferred into 35% PEG550 MME, 50 mM $ZnSO_4$, and 100 mM MES buffer, pH 6.5 for 10 s, native crystals were soaked for 15 min in 100 mM NO_2^- in 1.8 M lithium sulfate, and Na-acetate buffer, pH 4.25, N90S crystals were soaked for 30 s in 200 mM NO_2^- in 1.8 M lithium sulfate in citrate buffer pH 4.6. 1.8 M lithium sulfate was an effective cryoprotecting agent, preventing ice formation.

Crystallographic data were collected on the Soleil beamline PROXIMA1 using an ADSC 315 CCD detector to 1.46, 2.35, and 3.0 Å resolutions for the double mutant, native + NO_2^-, and N90S + NO_2^- structures, respectively. Data were integrated and scaled using XDS.[21] Double mutant and native + NO_2^- structures were solved by molecular replacement using PHASER[22] in the CCP4[23] program suite using PDB entry 1oe1 as the search model. The N90S + NO_2^- structure was refined starting from the isomorphous native + NO_2^- model. The structures were refined using REFMAC5[24] in the CCP4 program suite. For the double mutant, anisotropic temperature factors were refined and riding hydrogen atoms were added to the model. The native + NO_2^- structure was refined with isotropic *B*-factors and hydrogen atoms in riding positions. Rebuilding of the model between refinement cycles and adding waters was performed in Coot.[25] The lower resolution N90S + NO_2^- structure was refined with isotropic *B*-factors, and NCS constraints were applied to protein atoms in the 6 chains, excluding a flexible loop consisting of 8 residues (131−138). No NCS restraints were applied to metal or ligand atoms, and no bond length restraints were used for metal−ligand distances. It was not possible at the resolution of these structures to refine the occupancy of the nitrite molecule so this was set to 1 based on comparison of the *B*-factors of nitrite and surrounding residues. The crystal structures of N90S and H254F *Ax*NiR taken from ref 9 were rerefined against the original data using the same software as described above.

The quality of the models was assessed using Coot,[25] Procheck,[26] and the Molprobity[27] server. A summary of data and refinement statistics and the quality indicators for the structures are given in Table 1. Anomalous data sets for the N90S−H254F crystal were collected at wavelengths of 1.22 and 1.33 Å to determine Cu occupancy directly in each site in the crystals (see Supporting Information).

RESULTS AND DISCUSSION

Spectrochemical, Kinetic, and Proton Determination. *Cu Content of Recombinant Proteins.* The total Cu contents of recombinant native, N90S, H254F, and N90S−H254F *Ax*NiR, estimated spectrophotometrically, were 4.5 ± 0.9 Cu atoms per trimer for native *Ax*NiR, 4.3 ± 0.2 for N90S, 3.8 ± 0.2 for H254F, and 2.7 ± 0.2 for N90S−H254F. Six Cu atoms per *Ax*NiR trimer are expected for fully metalated enzyme.[7] The X-band EPR spectra of wild-type *Ax*NiR and the three proton channel mutants clearly show the presence of oxidized T1 and T2Cu centers, though the T2Cu hyperfine signal is less intense in the mutants containing the H254F mutation (Figure 2). The Cu parameters for both Cu centers derived from the EPR spectra are summarized in Table S1 (Supporting Information). Analysis of the intensity of the Cu hyperfine lines of freshly oxidized protein preparations showed T2Cu content relative to that of T1Cu of 75% for recombinant native and N90S, 42% for H254F, and 36% for the N90S−H254F double mutant which is in good agreement with the values obtained from the spectrophotometric analysis. A low T2Cu content has been reported previously for H254F, which preferentially incorporates Zn in the T2Cu site, although partial Cu loading can be achieved by adding 1 mM $CuSO_4$ to the growth medium.[9] Attempts to increase the Cu content of the purified N90S−H254F mutant by extensive dialysis (>50 h) against a solution of 40 mM MES (2-(*N*-morpholino)ethanesulfonic acid), pH 6, containing 20 mM $MgCl_2$ and 1 μM $CuSO_4$ did not result in any increase in Cu occupation, nor did it result in any increase in activity (results not shown).

Proton Consumption. The nitrite-dependent proton consumption during turnover was determined in unbuffered KCl solution using phenol red as a pH indicator, which reflects the changes in proton concentration of the bulk solution. On consumption of protons by NiR turnover the absorption spectrum of phenol red will decrease at 432 nm and increase at 556 nm. A calibration experiment in which known amounts of hydroxide ions were added to the sample mixture without enzyme was performed to correlate absorption changes to the amount of protons consumed (Supporting Information Figure S1-A). The proton consumption was determined at various nitrite concentrations, and spectra were recorded until the absorbance change reached its maximum (Supporting Information Figure S1−B). Since at higher substrate concentrations the reversibility of nitrite reduction by NiR becomes more prominent,[28] the data points were subjected to a linear fit, which was extrapolated to zero [nitrite] in order to determine the number of protons consumed per nitrite molecule.

For wild-type *Ax*NiR and both the N90S and H254F single mutants the number of protons consumed per nitrite molecule is close to 2; for the N90S−H254F mutant a value just under 1.5 was found. Thus, all *Ax*NiR proton channel variants studied consume more than 1 proton during catalytic turnover, and protons are still able to reach the active site in the N90S−H254F double mutant. Previously, Brenner et al. reported the consumption of 2.0 ± 0.04 protons per nitrite molecule for wild-type *Ax*NiR, the first evidence that two protons are involved in the turnover of *Ax*NiR at pH 7.[17]

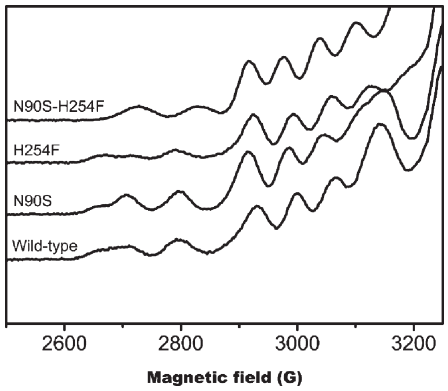

Figure 2. EPR spectra of wild-type *Ax*NiR and its proton channel mutants. Spectra were measured from 30 μM protein solutions in 25 mM MES−Hepes−maleic acid buffer, pH 7. Instrument conditions: temperature, 20 K; microwave frequency, 9.4 GHz; microwave power, 0.5 mW; modulation frequency, 100 kHz; and modulation amplitude, 5 G. Cu content of all samples was estimated using a Cu−EDTA standard assuming 100% T1Cu incorporation. Wild-type: 75% T2Cu occupancy; N90S: 75% T2Cu occupancy; H254F: 42% T2Cu occupancy; and N90S−H254F: 36% T2Cu occupancy.

Steady-State Kinetics. The steady-state kinetic activity of all four *Ax*NiR proton channel variants including native enzyme was determined in 50 mM potassium phosphate buffer, pH 7, at 4 °C using ascorbate as reducing agent and deoxyhemoglobin as NO scavenger. To ensure steady-state initial rate conditions for nitrite reduction as well as for NO scavenging, the assay was performed in a stopped-flow instrument by mixing enzyme and varying substrate concentrations with heme, excess reductant, and mediator (phenazine methosulfate). The heme absorbance changes upon NO binding to deoxyhemoglobin were monitored at 430 nm. The substrate dependence of the steady-state activity of wild-type *Ax*NiR and the three proton channel mutants are shown in Figure 3. Both wild-type *Ax*NiR and the H254F mutant follow Michaelis−Menten kinetics with substrate concentrations up to 10 mM. The apparent kinetic constants obtained by nonlinear fitting of the data gave similar values to those reported previously.[9,17] For wild-type *Ax*NiR an apparent K_M value of 26.8 ± 4.9 μM and an apparent k_{cat} of 89 ± 3 s^{-1} per monomer were found, and for H254F an apparent K_M of 30.8 ± 5.4 μM and an apparent k_{cat} of 44 ± 2 s^{-1} were found. The lower maximum velocity of the H254F variant is due to incomplete T2Cu incorporation. Both variants containing the N90S mutation, on the other hand, exhibit an unusual substrate inhibition pattern. At high nitrite concentrations the activity is inhibited, but the inhibition levels off and does not approach zero. Such an inhibition pattern could be explained by the presence of alternative routes in the reaction cycle, with the slower route becoming more dominant at higher substrate concentration, or by the binding of a second substrate molecule. However, we note that the latter has not been observed in crystal structures of any copper-containing NiR. Data obtained for *Ax*NiR N90S and N90S−H254F were fitted using the following equation:[29]

$$V_{obs} = \frac{\left(1 + \frac{b[S]}{K_i}\right) V_{max}}{1 + \frac{K_M}{[S]} + \frac{K_M}{K_i} + \frac{[S]}{K_i}} \quad (2)$$

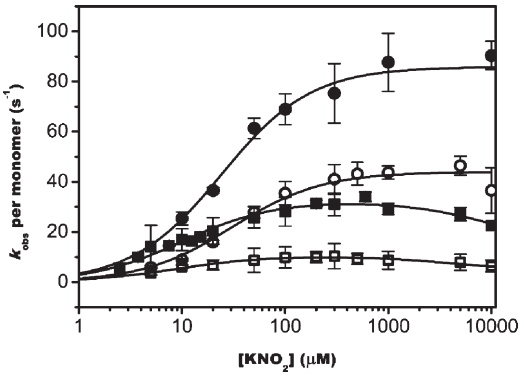

Figure 3. Substrate dependence of the steady-state activity of wild-type *Ax*NiR and its proton channel mutants, determined in 50 mM potassium phosphate buffer, pH 7 at 4 °C, using deoxyhemoglobin as NO scavenger (see Experimental Procedures). Initial rate data obtained for wild-type *Ax*NiR (black circles) and H254F (open circles) were fitted using the Michaelis−Menten equation. Data obtained for N90S (black squares) and the N90S−H254F double mutant (open squares) were fitted using eq 2. For clarity, the *x*-axis is presented on a logarithmic scale.

where *b* is the factor by which the maximum velocity is affected and the other symbols have their usual meaning. Fitting the data using eq 2 for both *Ax*NiR N90S and the N90S−H254F double mutant resulted in apparent K_M values of ∼10 μM, and a significantly reduced apparent k_{cat} of 32 ± 1 and 14 ± 1 s^{-1} per monomer for the single and double mutant, respectively. For both variants a *b* factor of ∼0.4 and a K_i in the millimolar range were found. All apparent kinetic parameters obtained from the nonlinear fits are summarized in Table 2.

When the experimental steady-state rates are corrected for T2Cu occupancy, both wild-type *Ax*NiR and H254F show ∼100% activity, and N90S and the N90S−H254F double mutant show ∼35% activity. These values are consistent with what has been shown previously for the H254F and N90S single mutants.[9]

Inter-Cu Electron Transfer. The inter-Cu ET from T1Cu to T2Cu in NiR can be followed by laser-flash photolysis experiments. Because the T1Cu is located just below the protein surface, it is much more readily reduced than the buried T2Cu. Following the fast initial reduction of T1Cu, resulting in a colorless Cu(I) state, the electrons redistribute between the two copper centers according to the thermodynamic equilibrium which is determined by the difference in the redox potentials of both copper centers.[13−15,17,30] In wild-type *Ax*NiR the reduction potentials of both copper centers presumably (since the potential of the T2Cu center has not previously been directly measured) have very similar values in the absence of substrate, providing little driving force for ET.[14,15] It is proposed that binding of the nitrite substrate increases the potential of the T2Cu center, thereby favoring ET from T1Cu to T2Cu during catalysis.[10,31,32] Because the T2Cu is effectively optically "silent" in either reduction state, only the redox state of the T1Cu can be monitored at 595 nm, allowing the inter-Cu ET to be studied.

All laser experiments were performed in 50 mM potassium phosphate buffer, pH 7, at 4 °C using NADH as artificial electron donor and *N*-methylnicotinamide as mediator. Kinetic traces obtained during the laser experiments were fitted to a double-exponential function:

$$\Delta A_{595} = A_0 + \Delta A_{1(obs)} e^{-k_1(obs)t} + \Delta A_{2(obs)} e^{-k_2(obs)t} \quad (3)$$

Table 2. Apparent Steady-State Kinetic Parameters for Wild-Type *Ax*NiR and the Three Proton Channel Mutants[a]

	K_M (μM)	k_{cat} (s^{-1})[b]	*b*	K_i (mM)
wild-type *Ax*NiR	26.8 ± 4.9	89 ± 3 (119 ± 4)[c]		
*Ax*NiR H254F	30.8 ± 5.4	44 ± 2 (105 ± 5)[c]		
*Ax*NiR N90S	10.0 ± 1.0	32 ± 1 (43 ± 1)	0.4 ± 0.1	10.4 ± 5.2
*Ax*NiR N90S−H254F	8.3 ± 2.0	14 ± 1 (39 ± 3)[c]	0.4 ± 0.1	5.1 ± 2.8

[a] Apparent kinetic constants were determined at 4 °C in 50 mM potassium phosphate buffer, pH 7, using excess reductant and deoxyhemoglobin as an NO scavenger. Values are presented as the mean ± SD of multiple experiments. Initial rate data obtained for wild-type *Ax*NiR and H254F were fitted using the Michaelis−Menten equation; data obtained for N90S and N90S−H254F were fitted using eq 2. [b] Per monomer. [c] Values corrected for partial T2Cu incorporation: 75% for wild-type *Ax*NiR and N90S, 42% for H254F, and 36% for N90S−H254F.

where $k_{1(obs)}$ and $k_{2(obs)}$ are the observed rate constants of T1Cu reduction and inter-Cu ET, respectively; $\Delta A_{1(obs)}$ and $\Delta A_{2(obs)}$ are the corresponding absorbance changes; *t* is the elapsed time after the flash; and A_0 is the offset absorbance value. The observed rates of inter-Cu ET are independent of T2Cu occupation in these single turnover experiments; this factor only affects the level of absorbance recovery in the absence of substrate.

As has been demonstrated previously in pulse-radiolysis and laser flash-photolysis experiments for wild-type *Ax*NiR,[14,15,17,30,33] following the initial fast reduction (∼3000−3500 s^{-1}) of T1Cu, in the absence of substrate the electrons redistribute between the two copper centers, which can be observed as a fast initial drop in the absorbance at 595 nm and a slower partial recovery. In the presence of excess nitrite (10 mM), a full recovery of the T1Cu signal is obtained, indicating complete ET from T1Cu to T2Cu as the reduced T2Cu is reoxidized by the reduction of nitrite. The H254F mutant behaves similarly to the wild-type enzyme in both the absence and presence of nitrite, an initial fast reduction of the T1Cu center of ∼3000−3500 s^{-1}, but with slightly higher subsequent inter-Cu ET rates compared to wild-type *Ax*NiR (Figure 4). The lower signal recovery in the absence of substrate in this mutant when compared with wild-type *Ax*NiR is due to incomplete T2Cu occupancy. Both *Ax*NiR N90S and the N90S−H254F double mutant, however, show a different behavior; after the reduction of the T1Cu (∼2000−2500 s^{-1}) no subsequent recovery absorbance at 595 nm occurs due to the perturbation of the T1Cu site potential (see below). However, inter-Cu ET is observed in the presence of nitrite in these mutants (Figure 4) and is attributed to the increase in potential of the T2Cu site consequent on nitrite binding.

The substrate dependence of the inter-Cu ET was also studied for wild-type and the proton channel variants. Both wild-type *Ax*NiR and the H254F mutant show similar complex substrate dependence, with an initial drop in ET rates at low nitrite concentrations and an increase at higher nitrite concentrations (Figure 5). Similar substrate dependences have been reported before and could only be described phenomenologically in the absence of a kinetic mechanism.[17] Both *Ax*NiR N90S and the N90S−H254F mutant show a substrate dependence that is different from the wild-type enzyme but similar to the substrate dependences observed in steady-state assays. Inter-Cu ET cannot be rate limiting in wild-type *Ax*NiR and the H254F mutant because their steady-state activity and internal ET show different substrate dependencies. In both the N90S single mutant and the N90S−H254F double mutant, however, similar patterns of substrate dependence were observed in both steady-state and

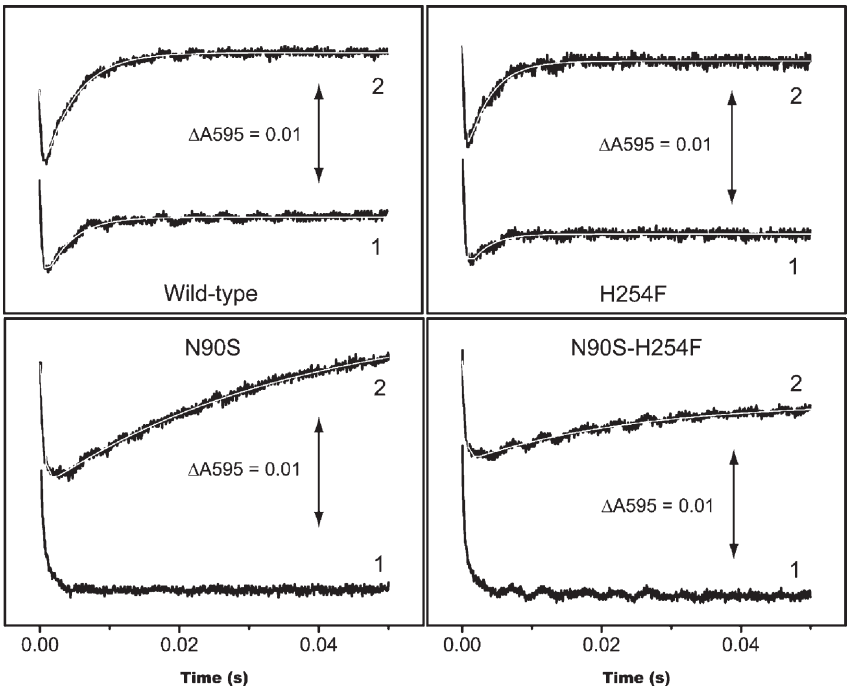

Figure 4. Absorbance changes at 595 nm observed in the laser-flash photolysis instrument during reduction of NiR with NADH (λ_{exc} = 355 nm). Experiments were carried out in 50 mM potassium phosphate buffer, pH 7, containing 30 μM NiR, 200 μM NADH, and 50 mM mediator at 4 °C. Traces shown are obtained in the absence (1) and in the presence of 10 mM nitrite (2). Traces were fitted using eq 3 (gray lines). Observed rates of ET, in the absence and presence of 10 mM nitrite, are respectively 266 and 217 s^{-1} for wild-type and 356 and 283 s^{-1} for H254F. Observed rates of ET for N90S and the double mutant in the presence of 10 mM substrate were 42 s^{-1} for both mutants. Note that the lack of recovery of absorbance at 595 nm for variants with the N90S substitution in the absence of nitrite indicates that no ET occurs unless substrate is present.

inter-Cu ET, suggesting that ET may be the rate-limiting step in these mutants. Previously, it was shown that inter-Cu ET is kinetically coupled to proton transfer;[17] therefore, proton transfer is likely to be rate-limiting in *Ax*NiR N90S and N90S−H254F. This indicates that the "Asn90" channel is the main source of protons to the active site of *Ax*NiR, but protons can still "leak" in the N90S single mutant and N90S−H254F double mutant, and this step becomes rate-limiting if the Asn90 channel is disrupted.

Reduction Potentials. To determine whether the altered inter-Cu ET behavior of N90S in the absence of substrate is caused by a thermodynamic effect, the reduction potentials of both copper centers in all three *Ax*NiR proton channel variants and the recombinant native enzyme were determined. UV−vis absorption spectra were recorded after each addition of dithionite to the oxidized protein, and a sample was withdrawn for EPR analysis. The reduction potentials for the T1Cu centers were estimated from the absorbance changes at 595 nm, while the reduction potentials for the T2Cu centers were estimated from the area under the T2Cu hyperfine peaks of the EPR spectra (see Supporting Information Figure S2).

The reduction potentials obtained from the fitted data are summarized in Table 3. Reduction potentials of +255 and +244 mV were found for the T1Cu and T2Cu in wild-type *Ax*NiR, respectively, similar to the values of +256 and +238 mV found for T1Cu and T2Cu centers, respectively, in H254F. This small difference in redox potentials between T1Cu and T2Cu provides very little driving force for ET in the absence of substrate. The obtained redox potentials are similar to previously published values for T1Cu and T2Cu in *Ax*NiR and *A. cycloclastes* NiR at pH 7.[14] No significant change in reduction potential was found for the T2Cu center of either N90S or N90S−H254F, which have values of +229 and +234 mV, respectively, but the T1Cu reduction potentials in these mutants were found to have increased by ~60 mV, resulting in a T1Cu reduction potential of +315 mV. This increase in T1Cu reduction potential results in a decreased driving force for inter-Cu ET, whereby ET becomes unfavorable in the absence of nitrite in *Ax*NiR variants N90S and N90S−H254F. Consistent with this, no inter-Cu ET was observed in these mutants in the absence of substrate (Figure 4). We note that a similar shift in the reduction potential of the T1Cu in *Ax*NiR M144A also resulted in a 70% decrease in activity.[30] The observed inter-Cu ET in the presence of substrate in the *Ax*NiR N90S and N90S−H254F mutants strongly suggests that the reduction potential of the T2Cu is increased upon binding of nitrite, in agreement with computational data.[16]

Crystal structures. *Crystal Structure of N90S−H254F.* The crystal structure of N90S−H254F was determined to 1.46 Å resolution Table 1. The rms deviations in Cα positions following superposition of the structure with the 1.04 Å recombinant native *Ax*NiR structure (PDB accession number 1oe1) were 0.22 Å for monomer A and 0.23 Å for monomer B. The N90S and H254F mutations are apparent from the electron density maps (Figure 6, Supporting Information Figure S3), and the structure near to these residues is essentially similar to that in the previously described N90S and H254F single mutant structures.[9] In order to ensure an accurate comparison, we also rerefined the single mutant structures from[9] using the same software as used for N90S−H254F (Table 1). Henceforth, references to the N90S and H254F single mutant structures refer to these rerefined coordinates. The single and double mutant crystal structures are isomorphous. There is no hydrogen bonding between Ser90 and Asp107, and the absence of two hydrogen bonds from residue

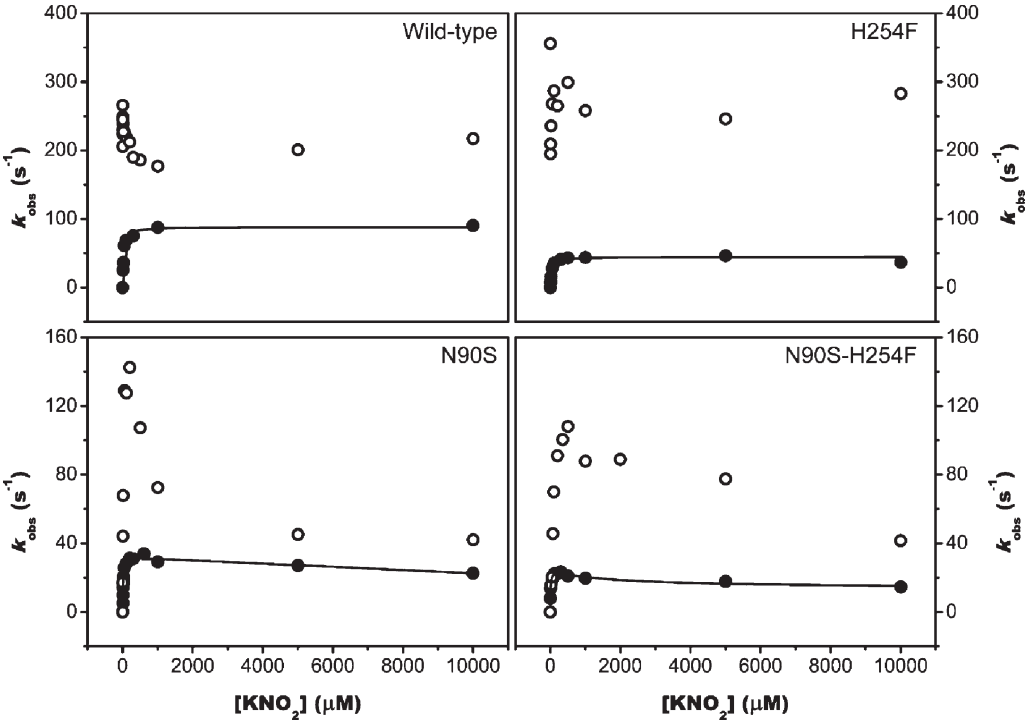

Figure 5. Substrate dependence of the inter-Cu ET compared to the rate of turnover during steady state. All experiments were carried out in 50 mM potassium phosphate buffer, pH 7, at 4 °C. Open circles: rate of inter-Cu ET determined by laser-flash photolysis; closed circles: rate of turnover per second per monomer during steady state (see Table 2 and Figure 4).

Table 3. Measured Reduction Potentials for Both Cu Centers in Wild-Type *Ax*NiR and Its Proton Channel Mutants[a]

variant	T1Cu (mV) vs SHE	T2Cu (mV) vs SHE
wild-type *Ax*NiR	255 ± 3	244 ± 18
H254F	256 ± 3	238 ± 5
N90S	315 ± 3	229 ± 5
N90S−H254F	315 ± 2	234 ± 7

[a] Redox titrations were performed in 50 mM potassium phosphate buffer, pH 7, at 25 °C. T1Cu reduction potentials were determined from the difference in absorbance at 595 nm between oxidized and reduced T1Cu, and T2Cu reduction potentials were determined from the difference in the hyperfine peaks of the EPR spectrum between oxidized and reduced T2Cu (see Supporting Information Figure S2).

His254 disrupts the hydrogen-bonding network; thus, in the double mutant both putative proton channels have been disrupted.

Anomalous diffraction data were measured to discriminate between Cu and Zn ions present at the T1 and T2Cu centers of N90S−H254F crystals (Supporting Information Figure S4 and Table S2). The data indicate low Cu loading at the T2Cu site in the crystal (∼10−20%) and full Cu loading of the T1Cu site, consistent with the EPR data (see below). Bond lengths and angles for the T1Cu site are given in Supporting Information Table S3. The first sphere coordination geometry is essentially unchanged as a result of the double mutation. Comparison of the N90S−H254F structure with that of recombinant native and the re-refined N90S and H254F single mutants indicates that the overall stereochemistry as well as bond distances of the inner sphere remain unaltered through mutations. However, a significant structural change occurs around Pro132, a residue that forms part of the "second sphere" surrounding the T1Cu center (Figure 7). In native *Ax*NiR this proline lies in close proximity to Asn90 and on mutation of Asn90 undergoes a position shift such that it moves somewhat toward the smaller side chain of Ser90 and away from the T1Cu ligand His139. This structural change in the N90S−H254F and N90S mutants may be a determining factor in their altered redox potentials. Previously, similar influences on redox potentials have been observed from the outer sphere residues in cupredoxins including azurins and rusticyanin.[34−36] We note that mutation of the second sphere residue Ser86 to Asp in rusticyanin from *Thiobacillus ferrooxidans* produced a change in redox potential of −44 mV.[36]

The T2Cu center of N90S−H254F has been modeled at full metal occupancy with a mixture of 0.2 Cu and 0.8 Zn ions, in a proportion slightly higher than estimated from the anomalous data (0.1/0.9) in order to enable a stable refinement. The Cu and Zn ions refine to positions ∼0.25 Å apart (Supporting Information Table S4).[a] A full-occupancy water molecule is present, ligated to the ion(s) occupying the T2Cu center at distances for chain A/B of ∼1.7/2.0 Å (to Cu) and ∼1.9/1.8 Å (to Zn). The close similarity of the T2Cu site in the N90S−H254F and N90S mutants implies that the structural/functional origin of the lowered K_M in these mutants is not the result of changes to the T2Cu environment in the substrate-free enzyme.

Crystal Structures of Nitrite-Soaked Native AxNiR and the N90S Mutant. There is very limited structural information for substrate binding in *Ax*NiR due to the difficulties of soaking the substrate into the most readily obtainable crystal form. Recently, we have been able to obtain $P2_12_12_1$ crystals that have proved amenable to soaking, unlike the *R*3 crystal form reported here and in ref 9, but unfortunately, the soaking of substrate results in a significant deterioration in the resolution. Despite this, it has

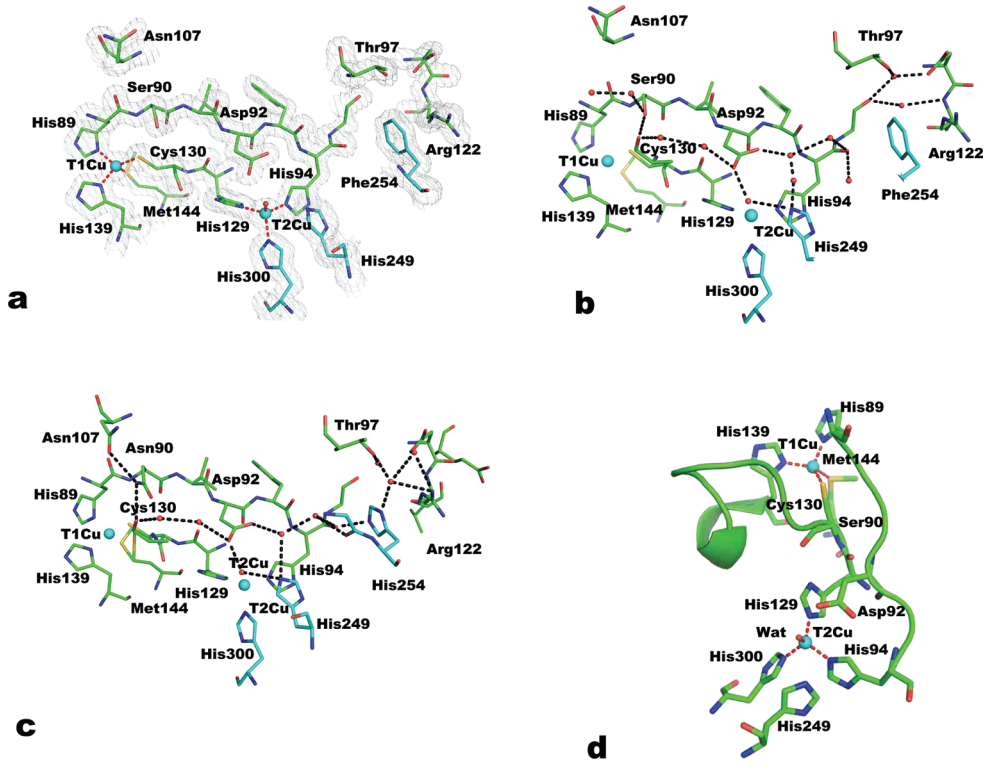

Figure 6. (a) $2F_o - F_c$ electron density map for *Ax*NiR N90S−H254F around residues Phe254 and Ser90 contoured at the 1σ level. Distances from Cu atoms to coordinating protein atoms are shown as dotted red lines. There are no significant structural changes in Ser90 (His254) sites to the corresponding site in the N90S (H254F) single mutant structures. (b) H-bonding networks for both proton channels in the N90S−H254F mutant are shown in gray dashed lines. (c) H-bonding networks for both proton channels in native *Ax*NiR are shown in gray dashed lines. Carbon atom bonds are shown in green for chain A and light blue for chain B for (a, b, c). (d) Sensor loop regions in the N90S−H254F mutant structure: Asp92-His89, His94-His89, and Cys130-His139.

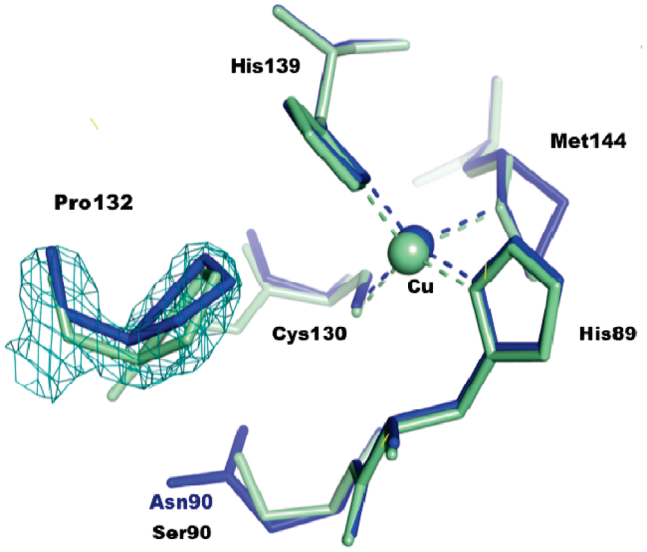

Figure 7. Superposition of the T1Cu center environment in recombinant native *Ax*NiR (blue) and N90S−H254F (pale cyan). On mutation of Asn90 to Ser, Pro132 is shifted toward the Ser90 side chain and somewhat away from His139 with possible consequences for T1Cu redox potential. Note that Pro 132 adopts the "native" conformation in the H254F structure and the shifted conformation in the N90S single mutant. The omit $2F_o - F_c$ electron density map for the *Ax*NiR N90S−H254F mutant around residue Pro132 contoured at the 1σ level is shown in cyan.

Table 4. Averaged Interatomic Distances[a] (Å) for T2Cu-Coordinated Nitrite and NO Molecules in the Native−NO_2^- and N90S−NO_2^- Structures

	A/B/D/F native−NO_2^-	C/E[b] native−NO_2^-	A/B/C/D/E/F N90S−NO_2^-
Cu−N (NO_2^-)	1.8	2.00	2.35
Cu−O2(NO_2^-)	1.95	2.0	2.0
Cu−O1(NO_2^-)			2.45
Asp92Oδ2−O2(NO_2^-)	2.6	2.75	3.1
His94Nε2−O2(NO_2^-)	2.9	3.15	3.0
His249Nε2−O2(NO_2^-)	2.95	3.05	2.9
Asp92Oδ2−N(NO)		3.3	

[a] Distances in separate monomers were refined independently and then averaged. Nitrite molecules were modeled with full occupancy. [b] Distances to O and N of NO.

allowed us to investigate the effect of the mutations upon substrate binding. Structures were determined from nitrite-soaked crystals of recombinant native (native + NO_2^-) and the N90S mutant (N90S + NO_2^-) of *Ax*NiR to 2.34 and 3.0 Å resolution, respectively, with two trimers in the crystallographic asymmetric unit (Tables 1 and 4). The rms deviations in Cα positions following superposition of the corresponding[b] chains of the native−NO_2^- structure to that of N90S−NO_2^- were between 0.22 and 0.57 Å. The monomers with the largest rms deviation (A, B) showed a maximum displacement of ~5 Å for residues

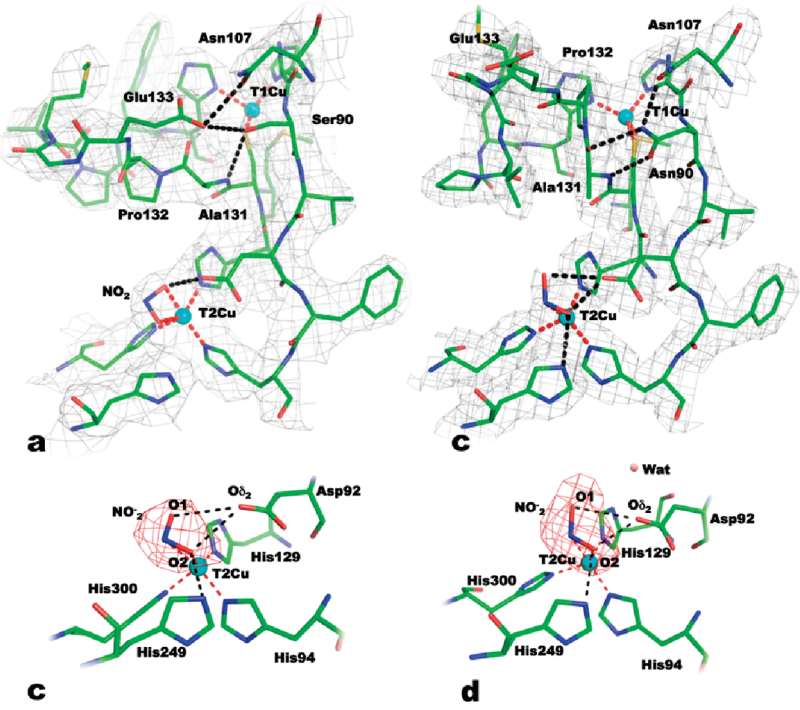

Figure 8. $2F_o - F_c$ electron density maps contoured at 1σ for N90S + NO_2^- chain C (a) and recombinant native + NO_2^- *Ax*NIR chain A (b). The Cu atoms are shown as cyan spheres with coordination bonds shown as dashed red lines. Important hydrogen bonds are shown as dashed black lines. The Ala131-Met138 loop undergoes a structural rearrangement in the N90S mutant upon nitrite binding, in contrast to native *Ax*NiR where no such loop movement was observed. The mode of nitrite binding is somewhat different in the N90S structure to the native enzyme (Table 4, see Supporting Information Figure S6). Electron density $F_o - F_c$ omit map contoured at 6σ for N90S + NO_2^- chain A (c) and recombinant native *Ax*NIR chain F (d).

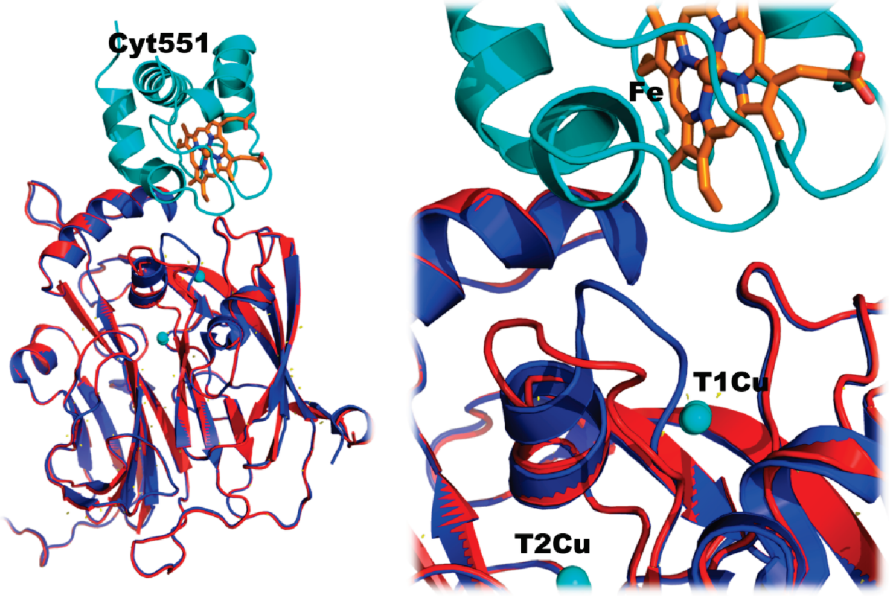

Figure 9. Superposition of the nitrite-bound native structure (in blue) with the nitrite-bound N90S structure (in red) and cytochrome−*c*551 (in cyan) from the cytochrome−NIR complex.[38] The zoom window shows the details of the 131−138 loop movement on nitrite binding in the mutant, a shift that was not observed in the native + NO_2^- structure.

Gly134 and Met135. These residues are part of the loop that connects Cys130 and His139, two of the T1Cu ligands.

The native + NO_2^- structure shows nitrite to be coordinated to T2Cu as a fourth ligand in four of the six monomers (A/B/D/F) (Figure 8b,d, Supporting Information Figure S5) while the remaining two molecules, C and E, have the product NO bound. It has previously been shown that X-rays can rapidly reduce the T1Cu in *Ax*NiR during data collection, resulting in the conversion of some of the nitrite to NO at the T2Cu site via internal ET.[37] The N90S mutant structure shows nitrite at the

dx.doi.org/10.1021/bi200246f |*Biochemistry* 2011, 50, 4121–4131

T2Cu site in all monomers (Figure 8a,c, Supporting Information Figure S5).

In the native + NO_2^- structure, nitrite is coordinated to T2Cu with its N and O2 atoms coordinated to Cu at 1.80 and 1.95 Å, respectively (Table 4). The O2 atom of nitrite is hydrogen-bonded to residues Asp92, His94, and His249, while the O1 atom of nitrite forms a H-bond with Asp92. A superposition of the native−NO_2^- structure with the substrate-free native structure (1oe1) shows a small shift in the position of Asp92 away from the nitrite. In the lower resolution N90S + NO_2^- structure, the Cu−nitrite N and O distances are 2.35 and 2.00 Å, respectively. The nitrite molecule is again hydrogen-bonded to residues Asp92, His94, and His249 (Table 4). In those monomers of the native + NO_2^- structure where NO is present, the distances from T2Cu to N and O are equal at 2.0 Å. A comparison of nitrite binding in these structures with that in previous *Ax*NiR and the green *Ac*NiR structures is given in (Supporting Information Figure S6).

Restoration of Proton Delivery via the Complex-Forming Loop. The most remarkable difference between the native and N90S nitrite-bound structures is in the conformation of the loop region between residues Ala131 and Met138 (Figures 8 and 9). The conformational change is more pronounced in chains B and C, while chains E, F have native-like conformation and A, D have both conformations present. Thus, each trimer has half of the molecules in the altered conformation. The chains with identical names have identical crystal surroundings in both nitrite-bound structures. The shift in position of the loop closes the NO_2^- binding pocket and exposes the T1Cu site for external interactions. Notably, residue Pro132 is moved out of the second coordination sphere in this new loop conformation. The slightly altered position of this residue in the substrate-free N90S and N90S−H254F structures (vide infra) suggests that this change could be the "trigger" for the loop movement. Notably this loop has been shown crystallographically to be involved in the formation of a potential electron transfer complex between Cyt_{551} and NiR,[38] and mutation and truncation of the residues in this loop causes a loss of catalytic activity and 200 mV increase in redox potential of the T1Cu site in *Ax*NIR.[39] This altered loop conformation in the substrate-bound N90S structure introduces a hydrogen bond network between Ser90 and the nearby Glu133 and Asn107 residues. This partially restored network could function as a proton channel, and this may provide a rationale for the retention of some catalytic activity in the N90S and N90S−H254F mutants. In addition, the "closed" conformation of the loop in the N90S + NO_2^- structure may cause a reduction in the ability of NO to escape the T2Cu site consistent with a lowered K_M value.

CONCLUSIONS

A detailed kinetic and structural analysis of three *Ax*NiR proton channel mutants—N90S, H254F, and the N90S−H254F double mutant—revealed that the Asn90 channel is the main proton delivery route in *Ax*NiR, but protons can still "leak" to the active site if this channel is disrupted. This may be facilitated by a population of the altered loop conformation in the substrate-bound structure, which introduces a hydrogen bond network between Ser90 and the nearby Glu133 and Asn107 residues. The steady-state kinetic activity for H254F is similar to wild-type but is reduced to ∼35% in N90S and N90S−H254F. In H254F and wild-type enzyme, electrons enter at the level of the T1Cu and then redistribute between the two Cu sites. Complete ET from T1Cu to T2Cu occurs only when nitrite binds at the T2Cu site. This indicates that substrate binding to T2Cu promotes ET from T1Cu, suggesting that the enzyme operates an ordered mechanism. Mutation of Asn90 in both the single and double mutants results in an increased redox potential (∼60 mV) for the T1Cu site, which is sufficient to completely abolish the ET between the Cu sites in the absence of the nitrite substrate. The effective ET in the case when nitrite binds clearly indicates that the redox potential of the T2Cu site is increased by at least 60 mV, further confirming that the two redox centers operate as a "coupled-potential" system. The loop connecting the T1Cu ligands Cys130 and His139 appears to be of key importance in restoration of the proton delivery in N90S and N90S−H254F, regulating the redox potential as well as in the formation of an ET complex between NiR and its redox partner protein.

ASSOCIATED CONTENT

Supporting Information. Experimental procedures for anaerobic sample preparation and Cu analysis, tables showing Cu EPR parameters, anomalous data collection statistics for the double mutant and Cu−ligand distances, and figures of the proton consumption determination and Cu redox potentials as well as additional figures showing stereoviews of Figures 6a and 8, an anomalous scattering difference map for the double mutant, and a superposition of the T1Cu environment of native *Ax*NiR and the double mutant. This material is available free of charge via the Internet at http://pubs.acs.org.

AUTHOR INFORMATION

Corresponding Author

*E-mail s.s.hasnain@liv.ac.uk, phone +44 151 795 5149, fax +44 151 795 5151 (S.S.H.); e-mail nigel.scrutton@manchester.as.uk, phone +44 161 306 5152, fax +44 161 306 8918 (N.S.S.).

Funding Sources

This work was supported by grants from the UK Biotechnology and Biological Sciences Research Council (BB/D016290/1 to S.S.H. and BB/G005850/1 to N.S.S.). N.S.S. is a BBSRC Professorial Research Fellow and a Royal Society Wolfson Merit Award holder.

ACKNOWLEDGMENT

We are grateful to SOLEIL and its staff for the provision of beamtime at PROXIMA-1. We acknowledge the support provided via the European TNA programme.

ABBREVIATIONS

*Ax*NiR, *Alcaligenes xylosoxidans* nitrite reductase; EPR, electron paramagnetic resonance; ET, electron transfer; NiR, nitrite reductase; NO, nitric oxide; T1Cu, type 1 copper; T2Cu, type 2 copper.

ADDITIONAL NOTE

[a] Because of the low occupancy of Cu at the T2Cu center.

[b] Monomers in an identical position in the crystallographic asymmetric unit.

REFERENCES

(1) Zumft, W. G. (1997) Cell biology and molecular basis of denitrification. *Microbiol. Mol. Biol. Rev. 61*, 533–616.

(2) Averill, B. A. (1996) Dissimilatory nitrite and nitric oxide reductases. *Chem. Rev. 96*, 2951–2964.

(3) Antonyuk, S. V., Strange, R. W., Sawers, G., Eady, R. R., and Hasnain, S. S. (2005) Atomic resolution structures of resting-state, substrate- and product-complexed Cu-nitrite reductase provide insight into catalytic mechanism. *Proc. Natl. Acad. Sci. U.S.A. 102*, 12041–12046.

(4) Ellis, M. J., Dodd, F. E., Sawers, G., Eady, R. R., and Hasnain, S. S. (2003) Atomic resolution structures of native copper nitrite reductase from *Alcaligenes xylosoxidans* and the active site mutant Asp92Glu. *J. Mol. Biol. 328*, 429–438.

(5) Suzuki, S., Kohzuma, T., Shidara, S., Okhki, K., and Aida, T. (1993) Novel spectroscopic aspects of type 1 copper in *Hyphomicrobium* nitrite reductase. *Inorg. Chim. Acta 208*, 107–109.

(6) Ellis, M. J., Grossmann, J. G., Eady, R. R., and Hasnain, S. S. (2007) Genomic analysis reveals widespread occurrence of new classes of copper nitrite reductases. *J. Biol. Inorg. Chem. 12*, 1119–1127.

(7) Dodd, F. E., Hasnain, S. S., Abraham, Z. H., Eady, R. R., and Smith, B. E. (1997) Structures of a blue-copper nitrite reductase and its substrate-bound complex. *Acta Crystallogr., Sect. D: Biol. Crystallogr. 53*, 406–418.

(8) Wijma, H. J., Jeuken, L. J. C., Verbeet, M. P., Armstrong, F. A., and Canters, G. W. (2006) A random-sequential mechanism for nitrite binding and active site reduction in copper-containing nitrite-reductase. *J. Biol. Chem. 281*, 16340–16346.

(9) Hough, M. A., Eady, R. R., and Hasnain, S. S. (2008) Identification of the proton channel to the active site type 2 Cu center of nitrite reductase: structural and enzymatic properties of the His254Phe and Asn90Ser mutants. *Biochemistry 47*, 13547–13553.

(10) Strange, R. W., Murphy, L. M., Dodd, F. E., Abraham, Z. H., Eady, R. R., Smith, B. E., and Hasnain, S. S. (1999) Structural and kinetic evidence for an ordered mechanism of copper nitrite reductase. *J. Mol. Biol. 287*, 1001–1009.

(11) De Marothy, S. A., Blomberg, M. R., and Siegbahn, P. E. (2007) Elucidating the mechanism for the reduction of nitrite by copper nitrite reductase-A contribution from quantum chemical studies. *J. Comput. Chem. 28*, 528–539.

(12) Abraham, Z. H., Smith, B. E., Howes, B. D., Lowe, D. J., and Eady, R. R. (1997) pH-dependence for binding a single nitrite ion to each type-2 copper centre in the copper-containing nitrite reductase of *Alcaligenes xylosoxidans*. *Biochem. J. 324*, 511–516.

(13) Suzuki, S., Deligeer, S., Yamaguchi, K., Kataoka, K., Kobayashi, K., Tawaga, S., Kohzuma, T., Shidara, S., and Iwasaki, H. (1997) Spectroscopic characterisation and intramolecular electron transfer processes of native and type-2 copper depleted nitrite reductases. *J. Biol. Inorg. Chem. 2*, 265–274.

(14) Kobayashi, K., Tagawa, S., Deligeer, and Suzuki, S. (1999) The pH-dependent changes of intramolecular electron transfer on copper-containing nitrite reductase. *J. Biochem. 126*, 408–412.

(15) Farver, O., Eady, R. R., Abraham, Z. H., and Pecht, I. (1998) The intramolecular electron transfer between copper sites of nitrite reductase: a comparison with ascorbate oxidase. *FEBS Lett. 436*, 239–242.

(16) Ghosh, S., Dey, A., Sun, Y., Scholes, C. P., and Solomon, E. I. (2009) Spectroscopic and computational studies of nitrite reductase: proton induced electron transfer and backbonding contributions to reactivity. *J. Am. Chem. Soc. 131*, 277–288.

(17) Brenner, S., Heyes, D. J., Hay, S., Hough, M. A., Eady, R. R., Hasnain, S. S., and Scrutton, N. S. (2009) Demonstration of proton-coupled electron transfer in the copper-containing nitrite reductases. *J. Biol. Chem. 284*, 25973–25983.

(18) Dodd, F. E., Van Beeumen, J., Eady, R. R., and Hasnain, S. S. (1998) X-ray structure of a blue-copper nitrite reductase in two crystal forms. The nature of the copper sites, mode of substrate binding and recognition by redox partner. *J. Mol. Biol. 282*, 369–382.

(19) Ellis, M. J., Dodd, F. E., Strange, R. W., Prudencio, M., Sawers, G., Eady, R. R., and Hasnain, S. S. (2001) X-ray structure of a blue copper nitrite reductase at high pH and in copper-free form at 1.9 A resolution. *Acta Crystallogr., Sect. D: Biol. Crystallogr. 57*, 1110–1118.

(20) Dutton, P. L., Sidney, F., and Lester, P. (1978) Redox potentiometry: Determination of midpoint potentials of oxidation-reduction components of biological electron-transfer systems. *Methods Enzymol. 54*, 411–435.

(21) Kabsch, W. (2010) *Acta Crystallogr., Sect. D: Biol. Crystallogr. 66*, 125–132.

(22) McCoy, A. J., Grosse-Kunstleve, R. W., Adams, P. D., Winn, M. D., Storoni, L. C., and Read, R. J. (2007) Phaser crystallographic software. *J. Appl. Crystallogr. 40*, 658–674.

(23) CCP4. (1994) The CCP4 Suite: Programs for Protein Crystallography, *Acta Crystallogr. D50*, 760−763.

(24) Murshudov, G. N., Vagin, A. A., and Dodson, E. J. (1997) Refinement of macromolecular structures by the maximum-likelihood method. *Acta Crystallogr., Sect. D: Biol. Crystallogr. 53*, 240–255.

(25) Emsley, P., and Cowtan, K. (2004) Coot: model-building tools for molecular graphics. *Acta Crystallogr., Sect. D: Biol. Crystallogr. 60*, 2126–2132.

(26) Laskowski, R. A., MacArthur, M. W., Moss, D. S., and Thornton, J. M. (1993) PROCHECK: A program to check the stereochemical quality of protein structures. *J. Appl. Crystallogr.* 26.

(27) Davis, I. W., Leaver-Fay, A., Chen, V. B., Block, J. N., Kapral, G. J., Wang, X., Murray, L. W., Arendall, W. B., 3rd, Snoeyink, J., Richardson, J. S., and Richardson, D. C. (2007) MolProbity: all-atom contacts and structure validation for proteins and nucleic acids. *Nucleic Acids Res. 35*, W375–383.

(28) Wijma, H. J., Canters, G. W., de Vries, S., and Verbeet, M. P. (2004) Bidirectional catalysis by copper-containing nitrite reductase. *Biochemistry 43*, 10467–10474.

(29) Roberts, P., Basran, J., Wilson, E. K., Hille, R., and Scrutton, N. S. (1999) Redox cycles in trimethylamine dehydrogenase and mechanism of substrate inhibition. *Biochemistry 38*, 14927–14940.

(30) Farver, O., Eady, R. R., Sawers, G., Prudencio, M., and Pecht, I. (2004) Met144Ala mutation of the copper-containing nitrite reductase from *Alcaligenes xylosoxidans* reverses the intramolecular electron transfer. *FEBS Lett. 561*, 173–176.

(31) Pinho, D., Besson, S., Brondino, C. D., de Castro, B., and Moura, I. (2004) Copper-containing nitrite reductase from *Pseudomonas chlororaphis* DSM 50135. *Eur. J. Biochem. 271*, 2361–2369.

(32) Olesen, K., Veselov, A., Zhao, Y., Wang, Y., Danner, B., Scholes, C. P., and Shapleigh, J. P. (1998) Spectroscopic, kinetic, and electrochemical characterization of heterologously expressed wild-type and mutant forms of copper-containing nitrite reductase from Rhodobacter sphaeroides 2.4.3. *Biochemistry 37*, 6086–6094.

(33) Suzuki, S., Deligeer, Yamaguchi, K., Kataoka, K., Kobayashi, K., Tagawa, S., Kohzuma, T., Shidara, S., Iwasaki, H., Deligeer, and Deligeer. (1997) Spectroscopic characterization and intramolecular electron transfer processes of native and type 2 Cu-depleted nitrite reductases. *J. Biol. Inorg. Chem. 2*, 265–274.

(34) Berry, S. M., Baker, M. H., and Reardon, N. J. (2010) Reduction potential variations in azurin through secondary coordination sphere phenylalanine incorporations. *J. Inorg. Biochem. 104*, 1071–1078.

(35) Kukimoto, M., Nishiyama, M., Tanokura, M., Murphy, M. E., Adman, E. T., and Horinouchi, S. (1996) Site-directed mutagenesis of azurin from Pseudomonas aeruginosa enhances the formation of an electron-transfer complex with a copper-containing nitrite reductase from Alcaligenes faecalis S-6. *FEBS Lett. 394*, 87–90.

(36) Hall, J. F., Kanbi, L. D., Harvey, I., Murphy, L. M., and Hasnain, S. S. (1998) Modulating the redox potential and acid stability of rusticyanin by site-directed mutagenesis of Ser86. *Biochemistry 37*, 11451–11458.

(37) Hough, M. A., Antonyuk, S. V., Strange, R. W., Eady, R. R., and Hasnain, S. S. (2008) Crystallography with online optical and X-ray absorption spectroscopies demonstrates an ordered mechanism in copper nitrite reductase. *J. Mol. Biol. 378*, 353–361.

(38) Nojiri, M., Koteishi, H., Nakagami, T., Kobayashi, K., Inoue, T., Yamaguchi, K., and Suzuki, S. (2009) Structural basis of inter-protein electron transfer for nitrite reduction in denitrification. *Nature 462*, 117–120.

(39) Sato, K., Firbank, S. J., Li, C., Banfield, M. J., and Dennisson, C. (2008) The importance of the long type 1 copper-binding loop of nitrite reductase for structure and function. *Chem.—Eur. J. 14*, 5820–5828.